Master *Sciences de la Matière*
École Normale Supérieure de Lyon
Université Claude Bernard Lyon

Stage 2008/2009
M2 Physique fondamentale

Computation of meson masses on the lattice

Author:
Roman Welsing
Amselstrasse 8
D-46325 Borken
roman.welsing@desy.de

Supervisor:
Dr. Karl Jansen
NIC, DESY, Zeuthen
Platanenallee 6
D-15738 Zeuthen

Abstract

In this report we will present the computation of meson masses on the lattice.
To do so we first discuss the calculation of correlation functions from first principles by means of numerical methods. After a short introduction, we will address the lattice action we have used and how we can extract a physical mass, for the pion namely, from a correlation function. The correlator is given by a statistical expectation value over contractions of fermionic propagators, which we calculate.
We further investigate the use of stochastic methods. We discuss how to calculate a reliable error for the statistical and stochastic mean value and from the resulting error, that we present, we deduce how to optimize the use of the introduced methods.

KEYWORDS:

Quantum Chromodynamics, Lattice QCD, Wilson fermions, Twisted mass,
HMC algorithm, Pion mass, Stochastic sources, Jackknife error

Zeuthen(Berlin), August 31, 2009

Contents

1 Introduction

1.1 Purpose of the project

The subject of this report is to study and understand the computation of meson masses on the lattice. This we have achieved by the calculation of correlation functions from first principles by means of numerical methods [Section 2.1]. We have namely run a Hybrid-Monte-Carlo algorithm (HMC) [Appendix A] to create gauge field configurations distributed according to a Boltzman factor e^{-S}, given by the action S. Hence the correlator is given by a statistical expectation value over contractions of fermionic propagators, which we calculate analytically [Section 2.3]. They depend on the gauge fields and are obtained by inverting the lattice Dirac operator using the conjugate gradient method. We have considered the mass degenerate isospin triplet of pions $\pi^{0,\pm}$. In the twisted-mass formulation of lattice QCD flavour symmetry is broken and therefore the correlation functions of the $\pi^{\pm}$ and the π^0 differ by so called disconnected diagrams, which vanish in the continuum limit, where flavour symmetry is restored. The main task therefore consisted in the investigation of stochastic methods [Section 3.3] for the computation of the disconnected diagram contributions to the π^0 mass. The goal was to understand and optimize these methods regarding statistical errors in gauge fields compared to the stochastic noise and taking into account the computational cost and runtime [Sections 3.2 and 4]. Therefore the approach was quite general in view of a further investigation of disconnected diagrams of the $\eta\prime$ meson correlator, because the computation of the $\eta\prime$ mass [7] will be one of the major topics of my ongoing work for my diploma thesis. The $\eta\prime$ mass is of particular interest in QCD since its mass originates to a large extent from topological effects of the gauge fields.
From a practical point of view, after getting familiar with the existing code, I have started to compute the $\pi^{\pm}$ correlator in the twisted-mass formulation of lattice QCD [Section 2.2] on a $4^3 \times 8$ discrete space-time lattice. In order to do this I have evaluated the fermionic path integral [Section 2.3] obtaining the up and down quark propagators after Wick contracting the corresponding field operators in the correlation function. I have learned to use and modify existing packages for writing, reading and inverting standard point sources and have then implemented the code performing those contractions. When going to the case of the neutral π^0 sector I have found, in order to get reasonable errors, I would need stochastic methods [Section 3.3] to calculate the contributions from disconnected quark diagrams to the correlator function. Hence I have written my own code writing and reading stochastic sources and performing the inversions and contractions using scripts, namely adapted to a batch farm at DESY Zeuthen. Once I had understood those techniques, I have studied the dependence of error estimates on the number of gauge fields and stochastic sources [Section 4], quantifying the error by Monte-Carlo and jackknife error methods [Section 3.2]. I have implemented the corresponding code. After I had understood the uncertainties in the numerical computation it was my goal to show how to obtain a physical value for the pion mass. In general our observables are depending on lattice artefacts, such as finite size and cutoff-effects, so this will be achieved by calculating reliable pion masses at several lattice spacings and extrapolating to the continuum limit [Section 3.1 and Section 5].

Acknowledgements

I am happy to say, that I have received a lot of help during the great time I had at DESY Zeuthen.
I would therefore like to thank Karl Jansen, not only for his support and for accepting me as a student, but also for his incredible patience. I thank Dru Renner and Carsten Urbach for guiding me through the sometimes very dark woods of Lattice QCD. I also appreciate the help I have received from Simon Dinter, who always kept his good mood despite all my sometimes stupid questions.
Last but not least I would like to thank the teachers of the École Normale Supérieure de Lyon for their commitment and for their teaching enthusiasm for research as well. In particular I am grateful to Thierry Dauxois and Aldo Deandrea. Of course I must thank Edith Thurel a whole lot for she has solved all the not only bureaucratic problems a student and a foreigner sometimes has to face.
Anyway I appreciate the hospitality I have enjoyed in France.

1.2 A look at continuum QCD and its phenomenology

Historically one has first studied the structure of hadronic matter by colliding protons with protons. In such experiments one has found, that the corresponding cross section is in extremely good agreement with a model of non interacting quarks constituting the nucleon. On the other hand one has found a large rate of hard scattering processes with high transversal momentum (arising from a higher interaction energy) in proton electron collisions, which are especially sensitive to electric charge. Those two phenomena have resulted in the parton model. It consists in the assumption that nuclei are formed by a small number of point like partons, interacting only weakly via the strong interaction but having electric charge. This absence of strong interactions in the high energy regime, called **asymptotic freedom** is one of the most characteristic features of the physics of quarks.
The only asymptotically free field theories found to date are non-Abelian gauge theories, proposed by 't Hooft, Politzer, Gross and Wilczek in the 1970s as a candidate for the theory of strong interactions. The vector boson exchange particles, so called gluons, were found to be the key to the understanding of quarks and their interactions.
While Abelian gauge theories in general lead to a screening effect of the charge produced by the vacuum polarization, only non-Abelian gauge theories can have self interactions of the vector bosons which lead to a growth of the charge with distance called anti-screening. Hence at small distances, or high energies, the charge gets smaller, which leads to asymptotic freedom, while for low energies a phenomenon called quark **confinement** occurs: the charge grows larger and the strong interactions are gluing the quarks together.
Finally, once we accept that non-Abelian gauge theories can describe these phenomena, the question arises which correct gauge symmetry we want to choose. It turns out that the group SU(3) is most promising. The quarks are found to carry a colour charge, while hadronic matter is colourless, i.e. baryons and mesons are colour singlets.
Accordingly this theory is called QCD, **Quantum chromodynamics**.
The QCD Lagrangian is given by:

$$\mathcal{L}_{QCD} = -\frac{1}{4}[F_{B\mu\nu}F^{B\mu\nu}] + \sum_f [\bar{q}_f(i\gamma^\mu D_\mu - m_f)q_f] \tag{1}$$

Where we have omitted the sum over the eight members of the colour octet, denoted by B in the field strength, and f represents the quark flavour index (f= up, down, strange, charm, bottom, top) arising from the six Dirac terms for all quark fermions and $D_\mu = \partial_\mu - igA_\mu$ is the covariant derivative.
Quantum chromodynamics has a number of interesting properties, relevant for our understanding of hadronic spectra. Chiral invariance stands out in a most prominent place among them. For example let us consider only the light (up and down quark) sector. If we assume that the masses of the up and the down quark are zero $m_u = m_d = 0$, there is a global chiral symmetry leading to a conservation of the axial vector currents:

$$A^f_\mu = \bar{q}\gamma_\mu\gamma_5\frac{\tau^f}{2}q \tag{2}$$

where we have introduced SU(2) flavour generators τ for f=1,2,3.
In reality, however, the axial $SU(2)_A$ symmetry is broken. Thus the axial current conservation is violated by a term proportional to the mass m_π of the pion field (with flavour g):

$$< 0|\partial_\mu A^f_\mu|\pi^g >= -f_\pi m^2_\pi \delta_{fg} \tag{3}$$

This is called the PCAC hypothesis (Partially Conserved Axial Current).

Hence we see that the pion mass m_π is a direct measure of the breaking of the axial $SU(2)_A$ symmetry, so we can conclude that it is very important to determine the value of the pion mass m_π. Therefore the computation of the pion mass m_π from first principles lattice QCD simulations is exactly the topic of this work.

2 Lattice QCD

Since Kenneth Wilson in 1974 and then Michael Creutz and others have first established the formulation of Quantum Chromodynamics on the lattice, they have paved the way for the study of non-perturbative phenomena by means of numerical methods. Nowadays with increasing computational power, Lattice QCD promises to answer such questions as whether QCD can explain quark confinement, whether it predicts the correct hadron spectrum or also if it accounts for the phase transition to a quark-gluon plasma at sufficiently high temperatures.

2.1 Numerical Path integrals

Lattice QCD is Quantum Chromodynamics, the theory of quarks and gluons and their interactions, formulated on a discrete space-time lattice.
The starting point is to use Feynman's path integral approach to quantization. Since the Hamiltonian formalism works with non-commuting operators, this approach, which uses only classical fields, is more amenable to direct numerical calculations. Moreover the path integral formalism is symmetric between space and time and after Wick rotating from real to imaginary time establishes a close connection between Quantum Field Theory and Statistical Mechanics. This analogy proves itself to be valuable, because it allows for the use of well known methods from statistical mechanics.
The information of the quantum theory, for example of a scalar field ϕ, is contained in the Green functions:

$$G(x,y,z,...) =< \Omega|T(\phi(x)\phi(y)\phi(z)...)|\Omega >\,, \tag{4}$$

where Ω denotes the ground state. Their path integral representation is (by insertion of complete sets of states and use of the path integral representation of the propagator) found to be:

$$G(x,y,z,...) = \frac{\int \mathcal{D}\phi\phi(x)\phi(y)\phi(z)...e^{iS[\phi]}}{\int \mathcal{D}\phi e^{iS[\phi]}}\,, \tag{5}$$

where the action $S = -\frac{1}{2}\int d^4x\phi(x)(\Box + M^2)\phi(x)$ results from the classical equations of motion $(\Box + M^2)\phi(x) = 0$ by the action principle $\delta S = 0$. More generally also a potential $V(\phi(x))$ can be added, which is, however left out here. If we now, by Wick rotating in the complex plane, continue to imaginary time $x_0 \to -ix_4$ the Green functions of Minkowski space become in Euclidean space:

$$< \phi(x)\phi(y)\phi(z)... >= \frac{\int \mathcal{D}\phi\phi(x)\phi(y)\phi(z)...e^{-S_E[\phi]}}{\int \mathcal{D}\phi e^{-S_E[\phi]}}\,, \tag{6}$$

with the Euclidean action given by $S_E[\phi] = \frac{1}{2}\int d^4x\phi(x)(-\Box + M^2)\phi(x)$. The Green functions of Minkowski space therefore in Euclidean space take the well known form of correlation functions of Statistical Mechanics defined by the partition function $Z = \int \mathcal{D}\phi e^{-S_E[\phi]}$. One can show that after Wick rotating from real to imaginary time, this imaginary time takes the role of the inverse $\beta = \frac{1}{k_B T}$ of the temperature T in Statistical Mechanics.
By looking at the quantum mechanical propagator $Z_{fi} =< \phi_f|e^{-HT}|\phi_i >\sim \int \mathcal{D}[\phi]e^{-S[\phi]}$ we identify the partition function of this system to be:

$$Z = \int d\phi < \phi|e^{-HT}|\phi >= Tre^{-HT} = \int \mathcal{D}[\phi]e^{-S_E[\phi]}\,, \tag{7}$$

where from now on T denotes the time extent. And hence we deduce that also in the general case of our analogy we can replace the inverse Temperature β by the time extent T:

$$\beta\hat{=}T\,. \tag{8}$$

We have by now noticed from the representation of the correlation functions, that there is a very close connection between classical Statistical Mechanics and quantum theory, which is revealed by Feynman's path integral approach.

We can thus employ simulation techniques which have proven to be useful in Statistical Mechanics already. But first let us give a precise mathematical definition of what we have called a path integral, by introducing a lattice, i.e. by discretizing the Euclidean space-time with a lattice spacing "a". This is done by the following replacements:

$$x_\mu \to n_\mu a \tag{9}$$

$$\phi(x) \to \phi(na) \tag{10}$$

$$\int d^4x \to a^4 \sum_n \tag{11}$$

$$\Box\phi(x) \to \frac{1}{a^2}\hat{\Box}\phi(na) \tag{12}$$

$$D\phi \to \prod_n d\phi(na)\,, \tag{13}$$

where the dimensionless lattice Laplacean $\hat{\Box}$ is defined as:

$$\hat{\Box} = \sum_\mu (\phi(na + \hat{\mu}a) + \phi(na + \hat{\mu}a) - 2\phi(na))\,. \tag{14}$$

We can now obtain a path integral expression for the correlator which involves only the dimensionless quantities $\hat{\phi}_n = a\phi(na)$ and $\hat{M} = aM$:

$$< \hat{\phi}_n\hat{\phi}_m... >= \frac{\int \prod_l d\hat{\phi}_l \hat{\phi}_n\hat{\phi}_m...e^{-S_E[\phi]}}{\int \prod_l d\hat{\phi}_l e^{-S_E[\phi]}}\,, \tag{15}$$

where we have introduced the discretized Euclidean action:

$$S_E = -\frac{1}{2}\sum_{n,\hat{\mu}} \hat{\phi}_n\hat{\phi}_{n+\hat{\mu}} + \frac{1}{2}(8 + \hat{M}^2)\sum_n \hat{\phi}_n\hat{\phi}_n = \frac{1}{2}\sum_{n,m} \hat{\phi}_n K_{nm}\hat{\phi}_m\,, \tag{16}$$

with $K_{mn} = -\sum_{\mu=1}^4[\delta_{n+\hat{\mu},m} + \delta_{n-\hat{\mu},m} - \delta_{n,m}] + \hat{M}^2\delta_{n,m}$. These integrals can obviously be evaluated analytically. For example by considering the generating functional,

$$Z_0[J] = \int \prod_l d\hat{\phi}_l e^{-S_E[\phi]+\sum_n \hat{J}_n\hat{\phi}_n} = \frac{1}{\sqrt{detK}} e^{\frac{1}{2}\sum_{n,m} J_n K^{-1}_{nm} J_m} \tag{17}$$

we obtain the two-point function of scalar field theory as:

$$< \hat{\phi}_n\hat{\phi}_m >= (\frac{\delta^2}{\delta J_n \delta J_m} Z_0[J])_{J=0} = K^{-1}_{nm}\,. \tag{18}$$

Now let us briefly discuss the case of Quantum Chromodynamics. As in the case of the scalar field, for free fermionic fields the correlation functions are given by the path integral representation,

$$< \hat{\Psi}_\alpha(n)...\bar{\hat{\Psi}}_\beta(m)... >= \frac{\int \prod_{k,\gamma} \mathcal{D}\bar{\hat{\Psi}}_\gamma(k) \prod_{l,\delta} \mathcal{D}\hat{\Psi}_\delta(l)\hat{\Psi}_\alpha(n)...\bar{\hat{\Psi}}_\beta(m)...e^{-S_F}}{\int \prod_{k,\gamma} \mathcal{D}\bar{\hat{\Psi}}_\gamma(k) \prod_{l,\delta} \mathcal{D}\hat{\Psi}_\delta(l) e^{-S_F}}\,, \tag{19}$$

where the Ψ are the anticommuting fermionic 4-component fields which in the path integral formulation are represented by anticommuting Grassmann numbers and S_F is the corresponding Euclidean action. The correlation functions can always be derived from a generating functional,

$$Z[\eta,\bar{\eta}] = \int \mathcal{D}\bar{\hat{\Psi}} \int \mathcal{D}\hat{\Psi} e^{-S_F+\sum_{n,\alpha}[\bar{\eta}_\alpha(n)\hat{\Psi}_\alpha(n)+\bar{\hat{\Psi}}_\alpha(n)\eta_\alpha(n)]} = \det[K] e^{\sum_{n,m,\alpha,\beta} \bar{\eta}_\alpha(n) K^{-1}_{\alpha\beta}(n,m)\eta_\beta(m)}\,, \tag{20}$$

with Grassmann valued sources $\eta_\alpha(n)$ and $\bar{\eta}_\alpha(n)$.

In the general case, where we include interactions, the partition function of Quantum Chromodynamics has to include a path integral over gauge fields U. The gauge fields U are the quantum fields representing the exchange particles called gluons, carrying the colour charge in interactions of quarks. Therefore we introduce a kinetic term for the self interacting gluons, the gauge field action $S_G[U]$.
Overall we thus have deduced a partition function:

$$Z = \int \mathcal{D}U \int \mathcal{D}\bar{\hat{\Psi}} \int \mathcal{D}\hat{\Psi} e^{-S_G[U] - S_F[\hat{\Psi}, \bar{\hat{\Psi}}, U]} \,. \tag{21}$$

After integrating out the fermionic Grassmann valued part of the path integral [Section 2.3], the path integral $\int \mathcal{D}U$ over gauge fields still remains. We have found that the correlation functions can be derived from a partition function. Hence the calculation of an expectation value of an observable O in lattice QCD corresponds to the computation of an ensemble average over gauge fields:

$$< O >= \frac{\int \mathcal{D}U O e^{-S_{eff}[U]}}{\int \mathcal{D}U e^{-S_{eff}[U]}} \,, \tag{22}$$

with the effective action:

$$S_{eff}[U] = S_G[U] - \ln(\det K[U]) \,. \tag{23}$$

Here $S_G[U]$ is again the non-Abelian gauge field action on the lattice, and K is the kernel of the fermionic part of the action. Note that due to the Grassmann integration rules, in Equation (20) the determinant of K appears in the numerator, in contrast to the bosonic case, where there is an inverse square root of the determinant in the denominator. Of course in order to evaluate this path integral one would have to perform a very large number of integrations. For example if we consider 10^4 space-time lattice points for a SU(3) theory there are roughly 4 x 10^4 links between these lattice points each with 8 gauge field degrees of freedom, which gives us a number of 320000 integrations to be done. Hence for 10 integration steps we would have to calculate 10^{320000} terms, which is even in the quenched approximation $\det[K] = 1$ impossible [2]. The idea, is thus, as in Statistical Mechanics, to randomly draw gauge field configurations with a probability distribution,

$$P(U_k)\mathcal{D}U = \frac{e^{-S[U]}\mathcal{D}U}{\int \mathcal{D}U e^{-S[U]}} \tag{24}$$

given by the Boltzmann factor $e^{-S[U]}$ so that the ensemble average of O will simply be given by the mean value of the operator O evaluated for those configurations:

$$< O > \simeq \frac{1}{N} \sum_{i=1}^{N} O(U_i) \,. \tag{25}$$

In the literature this is often refered to as **Importance Sampling**.
Methods to obtain gauge field configurations distributed according to the Boltzmann factor are described in appendix A. Our algorithm of choice is the HMC. [Appendix A.2].
It is based on a Markov process [Appendix A.1] which produces a sequence of configurations, which are exactly distributed according to the desired Boltzmann factor.
One of the most important problems for numerical calculations is the computation of a reliable error for the above approximation (25). See [13] for example. We also discuss this issue in section 3.2, where we explain how to estimate the error with the jackknife method and where we also discuss autocorrelation effects which lead to underestimation of the error due to correlations in the Markov chain [Appendix A.1]. At this stage we only want to mention that two seperate configurations in the sequence created by the HMC, can be correlated, which effectively reduces the statistical number of independent data.

During the rest of this report we will no longer explicitly consider the gauge field action. As the gauge field action $S_G[U]$ is of numerical importance only, and because in practice gauge field configurations are computed for one and for all times only, we refer the interested reader to see Appendix B for further details. In the following we will limit ourselves to the formulation of the fermionic action on the lattice only.

2.2 Formulation of the lattice action

While we have seen that the formulation of scalar field theory on the lattice is unproblematic, we will now show that the task to put fermions on a discrete space-time lattice leads to difficulties. We use these ambiguities to illustrate that we have a freedom regarding which lattice action we want to choose, as long as it leads to the correct continuum limit. We will namely present the so called doubling problem. This problem arises when naively discretizing the fermionic part of the action. To illustrate this, let us consider the free Dirac field, which in Minkowski space obeys the Dirac equation

$$(i\gamma^\mu \partial_\mu - M)\Psi(x) = 0\,. \tag{26}$$

This equation of motion follows from an action, which in Euclidean space reads:

$$S_F[\Psi, \bar{\Psi}] = \int d^4x \bar{\Psi}(x)(i\gamma^\mu \partial_\mu + M)\Psi(x)\,, \tag{27}$$

where the Ψ are again the anticommuting fermionic 4-component fields which in the path integral formulation are represented by anticommuting Grassmann numbers.
In order to obtain dimensionless variables again, we substitute:

$$M \to \frac{1}{a}\hat{M} \tag{28}$$

$$\Psi_\alpha(x) \to \frac{1}{a^{3/2}}\hat{\Psi}_\alpha(n) \tag{29}$$

$$\bar{\Psi}_\alpha(x) \to \frac{1}{a^{3/2}}\bar{\hat{\Psi}}_\alpha(n) \tag{30}$$

$$\partial_\mu \Psi_\alpha(x) \to \frac{1}{a^{5/2}}\hat{\partial}_\mu \hat{\Psi}_\alpha(n)\,, \tag{31}$$

where $\hat{\partial}_\mu$, the antihermitian lattice derivative, is defined by:

$$\hat{\partial}_\mu \hat{\Psi}_\alpha(n) = \frac{1}{2}[\hat{\Psi}_\alpha(n+\hat{\mu}) - \hat{\Psi}_\alpha(n-\hat{\mu})]\,. \tag{32}$$

Therefore one gets for the naive lattice action,

$$S_F = \sum_{n,m,\alpha,\beta} \bar{\hat{\Psi}}_\alpha(n) K_{\alpha\beta}(n,m) \hat{\Psi}_\beta(m)\,, \tag{33}$$

where we have introduced,

$$K_{\alpha\beta}(n,m) = \sum_\mu \frac{1}{2}(\gamma_\mu)_{\alpha\beta}[\delta_{m,n+\hat{\mu}} - \delta_{m,n-\hat{\mu}}] + \hat{M}\delta_{mn}\delta_{\alpha\beta}\,. \tag{34}$$

Hence the correlation function from the generating functional [Equation (20)] is again found to be,

$$< \hat{\Psi}_\alpha(n) \bar{\hat{\Psi}}_\beta(m) >= K^{-1}_{\alpha\beta}(n,m)\,, \tag{35}$$

which by Fourier transformation becomes,

$$< \hat{\Psi}_\alpha(n) \bar{\hat{\Psi}}_\beta(m) >= \lim_{a\to 0} \int_{-\frac{\pi}{a}}^{\frac{\pi}{a}} \frac{d^4p}{(2\pi)^4} \frac{[-i\sum \gamma_\mu \tilde{p}_\mu + M]_{\alpha\beta}}{\sum_\mu \tilde{p}_\mu^2 + M^2} e^{ip(x-y)}\,, \tag{36}$$

where we have introduced $\tilde{p}_\mu = \frac{1}{a}\sin(p_\mu a)$ which in the continuum limit $a \to 0$ yields $\lim_{a\to 0} \tilde{p}_\mu = p_\mu$.

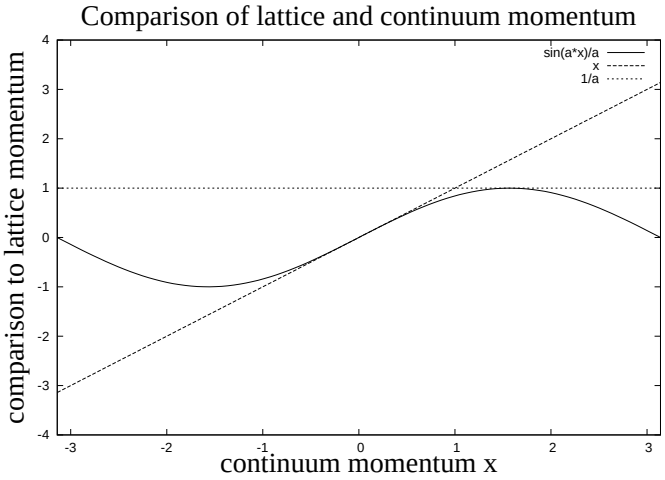

Figure 1: Plot of $\tilde{p}_\mu = \frac{1}{a} sin(p_\mu a)$ versus $x = p_\mu$ in the Brillouin zone $[-\frac{\pi}{a}, \frac{\pi}{a}]$
Correct continuum limit at $x = p_\mu \approx 0$ - Incorrect continuum limit at $x = p_\mu \approx \frac{\pi}{a}$

But this is only true for momenta p_μ contained in the center of the Brillouin zone

$$-\frac{1}{2}\frac{\pi}{a} < p_\mu < \frac{1}{2}\frac{\pi}{a} \tag{37}$$

as is shown in Figure 1. Here we can neglect the deviations near the maximum of the sine function, because there we have $\tilde{p}_\mu \sim \mathcal{O}(\frac{1}{a})$ and thus in the continuum limit all deviations are suppressed as $\tilde{p}_\mu$ is diverging in the denominator of Equation (36). However in the other parts of the Brillouin zone with momenta

$$p_\mu < -\frac{1}{2}\frac{\pi}{a}, \frac{1}{2}\frac{\pi}{a} < p_\mu \tag{38}$$

we can see a deviation of the lattice momentum $\tilde{p}_\mu$ from the continuum momentum p_μ for $a \to 0$. Note that in Figure 1 $\tilde{p}_\mu$ again yields a finite value at the corner of the Brillouin zone $p_\mu = \frac{\pi}{a}$, namely for $a \to 0$: $\tilde{p}_\mu = 0$, which is a clear difference.
Hence there are contributions to the integral Equation (36) above, given by the corners of the Brillouin zone. In 4 dimensions there is $2^4 = 16$ such corners (e.g. $[\frac{\pi}{a},0,0,0]$, $[0,\frac{\pi}{a},0,0]$, $[\frac{\pi}{a},\frac{\pi}{a},0,0]$, etc.) one doubling for each additional dimension, where we have included the origin. The zeros of the sine-function at these corners destroy the correct continuum limit as $\tilde{p}_\mu$ is finite for $a \to 0$. We thus have 15 additional fermion-like low momentum modes, which are pure lattice artefacts, actually arising from the fact, that the symmetric discretization of the derivatives involves twice the lattice spacing, giving rise to an additional solution with equal eigenvalue. This is called the **doubling problem**.
Of course we are free to choose a different action, given that in the continuum limit it leads to the same theory. We can thus modify our action by an additional term, first introduced by Wilson in 1975, which vanishes in the naive continuum limit. Wilson's action for fermions reads,

$$S_F^{(W)} = S_F - \frac{r}{2}\sum_n \bar{\hat{\Psi}}(n)\hat{\Box}\hat{\Psi}(n) = \sum_{n,m} \bar{\hat{\Psi}}(n) K_{\alpha\beta}^{(W)}(n,m)\hat{\Psi}_\beta(m)\,, \tag{39}$$

where

$$K_{\alpha\beta}^{(W)}(n,m) = (\hat{M} + 4r)\delta_{nm}\delta_{\alpha\beta} - \frac{1}{2}\sum_\mu [(r-\gamma_\mu)_{\alpha\beta}\delta_{m,n+\hat{\mu}} + (r+\gamma_\mu)_{\alpha\beta}\delta_{m,n-\hat{\mu}}]\,. \tag{40}$$

It is important to stress that in general the partial derivative is replaced by the covariant derivative and hence is depending upon the gauge fields.

Moreover we want to formulate a gauge invariant action. Due to the limited room in this report we discuss this issue in Appendix B and limit ourselves to discuss the free case in this section only.
Wilson's action, in the free case, leads again to the two-point function (36), with M replaced by,
$M \to M(p) = M + \frac{2r}{a}\sum_\mu \sin^2(p_\mu a/2)$, and where we still define $\tilde{p}_\mu = \frac{1}{a}\sin(p_\mu a)$.
Now we can see that in the limit $a \to 0$: $M(p) \to M$ except at the corners of the Brillouin zone where M(p) diverges. This eliminates the doubling problem, as the low momentum excited states are suppressed: $\sim \frac{1}{M(p)}$

One disadvantage of this method is that it breaks the chiral symmetry of the action for M=0. A further problem is that the kernel K can have eigenvalue zero. Therefore the fermionic determinant is equal or in numerical calculations close to zero, $\det[K] = 0$, which means that the according configuration for this propagator should have a statistical weight zero. But the propagator, the inverse of the Dirac operator, diverges. Such configurations which compromise the validity of our ensemble are called exceptional configurations. Hence there are various alternative attempts to formulate actions on the lattice.
In these attempts there is a choice to be made. We can sacrifice full chiral symmetry with the advantage of lower computational cost, or we can choose a rather complicated lattice action which keeps chiral symmetry, but which is of course harder to simulate.

One action which uses rather simple **Wilson type fermions** is the twisted-mass action. One virtue is that in **twisted-mass QCD** the exceptional configurations have been removed. Originally twisted-mass QCD is a scheme for a doublet of two flavours $N_f = 2$ where the Wilson type lattice Dirac operator D_W is replaced by:

$$D_{twist} = D_W + m_q + i\mu_q\gamma_5\tau_3\,. \tag{41}$$

The isospin operator τ_3 acts in flavor space and the parameter μ_q is called the twisted mass.
Now doublers are avoided, as we use Wilson type fermions and moreover exceptional configurations are removed for $\mu_q > 0$:

$$\det[D_{twist}] = \det[(D_W + m_q)^+(D_W + m_q) + \mu_q^2] > 0 \tag{42}$$

One can verify that the continuum twisted mass action,

$$S_F[\Psi,\bar{\Psi}] = \int d^4x\bar{\Psi}(x)(\gamma^\mu D_\mu + m_q + i\mu_q\gamma_5\tau_3)\Psi(x) \tag{43}$$

under a chiral rotation,

$$\chi = e^{i\gamma_5\tau_3\omega/2}\Psi \tag{44}$$

$$\bar{\chi} = \bar{\Psi}e^{i\gamma_5\tau_3\omega/2} \tag{45}$$

for $\tan(\omega) = \frac{\mu_q}{m_q}$ becomes,

$$S_F[\chi,\bar{\chi}] = \int d^4x\bar{\chi}(x)(\gamma^\mu D_\mu + M)\chi(x)\,, \tag{46}$$

where $M = \sqrt{m_q^2 + \mu_q^2}$.
While for non-zero lattice spacing the twisted-mass term breaks both flavour and parity symmetries, in the continuum limit these symmetries are restored. The breaking of the flavor symmetry leads to a mass splitting between charged and neutral pions. [Section 2.3] This is explicitly arising from additional contribution of disconnected loops to the correlator. These vanish in the continuum limit, where symmetries are restored with $\mathcal{O}(a^2)$ [Section 3.1] at **maximal twist**: $\omega = \frac{\pi}{2}$.
Thus one main advantage of Wilson twisted-mass lattice QCD is that at maximal twist we have automatic $\mathcal{O}$(a) improvement. In contrast standard Wilson fermions approach the continuum only at a rate of $\mathcal{O}$(a). Maximal twist can be obtained by tuning:

$$m_q \to m_q = 0 \Rightarrow \omega = \frac{\pi}{2}\,. \tag{47}$$

This, in practice, is achieved by setting the PCAC mass to zero.

$$m_{PCAC} = \frac{\sum_x < \partial_0 A_0^a(x)P^a(0) >}{2\sum_x < P^a(x)P^a(0) >} \tag{48}$$

2.3 Spectroscopy of pion masses

The ultimate goal of calculating correlation functions in lattice QCD is to extract values of physical observables such as masses from them. The most general two point correlation function of two observables O_i and O_j can in Statistical Mechanics be written,

$$C_{ij}(t) = Tr[O_i(t)O_j(0)e^{-\beta H}]/Z\,, \tag{49}$$

with the partition function given by $Z = Tr[e^{-\beta H}]$. Now as we have found $\beta \hat{=} T$, where T is the time extent and β the inverse of the temperature, we can write our two point correlation function as:

$$C_{ij}(t) = \frac{\sum_n e^{-E_n T} < n|O_i(t)O_j(0)|n >}{\sum_n e^{-E_n T}}\,, \tag{50}$$

which in the "zero temperature limit" $T \to \infty$ gives just the vaccuum expectation value:

$$\lim_{T\to\infty} C_{ij}(t) =< 0|O_i(t)O_j(0)|0 > \ . \tag{51}$$

After inserting a complete set of states we get by considering the time evolution $O_i(t) = e^{Ht}O_i e^{-Ht}$:

$$C_{ij}(t) = \sum_n < 0|O_i|n >< n|O_j|0 > e^{-(E_n - E_0)t}/Z\,. \tag{52}$$

Obviously in the large time limit for $t \to \infty$ the lowest energy states are dominating, which for i=j yields,

$$C_{ii} \simeq | < 0|O_i|0 > |^2 + | < 0|O_i|1 > |^2 e^{-(E_1 - E_0)t}\,, \tag{53}$$

Usually correlation functions are defined with the first vaccuum disconnected part removed:

$$C_{ii} \simeq | < 0|O_i|1 > |^2 e^{-(E_1 - E_0)t}\,, \tag{54}$$

Therefore the correlation length, which determines the exponential decay rate, is given by the inverse of the mass gap:

$$\zeta = (E_1 - E_0)^{-1} = \frac{1}{am}\,, \tag{55}$$

Now let us consider the field operator creating charged pions, which are pseudoscalar mesons:

$$\pi^{\pm} = \bar{d}\gamma_5 u\,. \tag{56}$$

Since we want to calculate the mass of the charged pion, this leads us directly to the two-point correlation function, which can be evaluated from the general case of the generating functional:

$$< \pi^+(x)\pi(y) >=< \bar{u}(x)\gamma_5 d(x)\bar{d}(y)\gamma_5 u(y) > \tag{57}$$

$$= \int \mathcal{D}U\mathcal{D}u\mathcal{D}\bar{u}\mathcal{D}d\mathcal{D}\bar{d}[\bar{u}\gamma_5 d\bar{d}\gamma_5 u]e^{\int(-\bar{u}G_u^{-1}u - \bar{d}G_d^{-1}d) + S_G}/Z \tag{58}$$

$$= \int \mathcal{D}U \det[G_u]\det[G_d]G_u(x,y)\gamma_5 G_d(y,x)\gamma_5 e^{-S_G}/Z \tag{59}$$

$$\Leftrightarrow < \pi^+(x)\pi(y) >=< \bar{u}(x)\gamma_5 d(x)\bar{d}(y)\gamma_5 u(y) > \ . \tag{60}$$

Here we have introduced the Wick contractions equivalent to the path integral.
With $\overbrace{u(x)\bar{u}(y)} = G_u(y,x)$ this leads to the propagator:

$$< \pi^+(x)\pi(y) >=< Tr[G_u(x,y)\gamma_5 G_d(y,x)\gamma_5] > \ . \tag{61}$$

Finally the field operator for the neutral pion, which is in a flavour singlet pseudoscalar state, in the twisted basis [Appendix D] reads:

$$\pi^0 = \frac{1}{\sqrt{2}}(\bar{u}u + \bar{d}d)\,. \tag{62}$$

Accordingly the two-point correlation function becomes:

$$< \pi^+(x)\pi(y) > = < \frac{1}{2}(\bar{u}(x)u(x) + \bar{d}(x)d(y))(\bar{u}(y)u(y) + \bar{d}(y)d(y)) > \tag{63}$$

$$= \frac{1}{2}[< \bar{u}(x)u(x)\bar{u}(y)u(y) > + < \bar{d}(x)d(x)\bar{d}(y)d(y) > \tag{64}$$

$$+ < \bar{d}(x)d(x)\bar{u}(y)u(y) > + < \bar{u}(x)u(x)\bar{d}(y)d(y) >] \tag{65}$$

$$= \frac{1}{2}[< \bar{u}(x)u(x)\bar{u}(y)u(y) > + < \bar{d}(x)d(x)\bar{d}(y)d(y) > \tag{66}$$

$$+ < \bar{u}(x)u(x)\bar{u}(y)u(y) > + < \bar{d}(x)d(x)\bar{d}(y)d(y) > \tag{67}$$

$$+ < \bar{d}(x)d(x)\bar{u}(y)u(y) > + < \bar{u}(x)u(x)\bar{d}(y)d(y) >]\,. \tag{68}$$

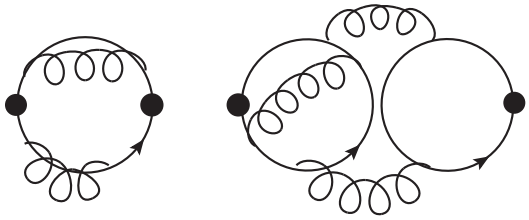

Figure 2: Connected and disconnected quark diagrams

Hence we still have the usual connected contributions now averaged over up and down quarks. But for non zero lattice spacing, i.e. with broken flavor symmetry, we have disconnected contributions as well.

$$< \pi^+(x)\pi(y) > = \frac{1}{2} < Tr[G_u(x,x)]Tr[G_u(y,y)] + Tr[G_u(x,y)G_u(y,x)] + Tr[G_d(x,x)]Tr[G_d(y,y)] \tag{69}$$

$$+Tr[G_d(x,y)G_d(y,x)] + Tr[G_u(x,x)]Tr[G_d(y,y)] + Tr[G_d(x,x)]Tr[G_u(y,y)] > \tag{70}$$

With the identity,

$$G_d(x,y) = \gamma_5 G_u^+(y,x)\gamma_5 \tag{71}$$

the disconnected contribution thus becomes,

$$D = \frac{1}{2} < Tr[G_u + G_u^+]Tr[G_u + G_u^+] > = 2 < (Tr[Re(G_u)])^2 >\,, \tag{72}$$

while for the connected contribution we had,

$$C = < Tr[G_u(x,y)\gamma_5 G_d(y,x)\gamma_5] > \ . \tag{73}$$

Keep in mind that in the end we will always consider the correlation function in momentum space at zero momentum, where we have summed over all space-volume dependences:

$$C(\vec{p},t) = \int d^3x e^{i\vec{p}\vec{x}} C(\vec{x},t,0,0) \tag{74}$$

$$C(t) = C(0,t) \simeq \sum_{\vec{x}} C(\vec{x},t,0,0)\,. \tag{75}$$

3 Simulation and Analysis Details

If we want to compare the experimental data for a physical observable to numerical results, one will always find lattice artefacts. One reason is the finite volume of the lattice. These are finite size effects. Another reason is the non zero lattice spacing leading to discretization errors, called cutoff-effects.

3.1 Cutoff-effects and improvement

In practice therefore in order to eliminate the cutoff-effects one will always calculate the physical entity for several lattice spacing, and extrapolate in dependence of the lattice spacing. We say that we take the continuum limit.
Hence because of our limited ability to approach the continuum it is often necessary to improve the discretization errors to $\mathcal{O}(a^2)$ to obtain a sufficient data set. One possiblity to achieve this is the Symanzik improvement program, another elegant way is to take advantage of automatic $\mathcal{O}(a)$ improvement of twisted-mass QCD at maximal twist. We shortly mention these techniques in Appendix C.

3.2 Monte-Carlo errors and jackknife

Another field of great practical significance is the comprehension of statistical standard errors. It is not possible to overstress the importance of the computation of reliable errors, in order to compare numerical results to experiment. To do this one first has to gain a comprehension of the goodness of our statistical Monte-Carlo ensemble, the gauge field configurations. One of the keys to make quantitative estimates of the statistical independence of our data set is the **autocorrelation** [9]. If we call our observable quantities a_α and accordingly their exact statistical mean values A_α the autocorrelation function is defined by:

$$\Gamma_{\alpha\beta}(i-j) =< (a^i_\alpha - A_\alpha)(a^j_\beta - A_\beta) > , \tag{76}$$

where a^i_α and a^j_α are at positions i and j in our sequence of Monte-Carlo generated samples [Appendix A]. In the case of the generation of configurations via the Hybrid-Monte-Carlo algorithm HMC this is often refered to as Monte-Carlo time τ. Now we take the mean value $\bar{a}_\alpha = \frac{1}{N}\sum_{i=1}^{N} a^i_\alpha$ as the natural estimator for the primary observables A_α and hence we get for the covariance matrix,

$$< (\bar{a}_\alpha - A_\alpha)(\bar{a}_\beta - A_\beta) >= \frac{1}{N^2}\sum_{i,j=1}^{N}\Gamma_{\alpha\beta}(i-j) \simeq \frac{1}{N}\sum_{t}\Gamma_{\alpha\beta}(t) \simeq \frac{1}{N}C_{\alpha\beta} + \mathcal{O}(\frac{1}{N^2}) , \tag{77}$$

where we have introduced:

$$C_{\alpha\beta} = \sum_{t=-\infty}^{\infty}\Gamma_{\alpha\beta}(t) . \tag{78}$$

This means that the error σ_α for the estimate of A_α is to leading order given by the estimate $\sigma^2_\alpha \simeq \frac{1}{N}C_{\alpha\alpha}$. By introducing the integrated autocorrelation time,

$$\tau^{int}_\alpha = \frac{1}{2v_\alpha}\sum_{t=-\infty}^{\infty}\Gamma_{\alpha\alpha}(t) \tag{79}$$

this estimate takes the form,

$$\sigma^2_\alpha = \frac{2\tau^{int}_\alpha}{N}v_\alpha , \tag{80}$$

where $v_\alpha = \Gamma_{\alpha\alpha}(0)$ is the naive variance, not taking into account autocorrelation effects. It is corrected for by a factor given by the integrated autocorrelation time and divided by the number of samples to give an accurate error estimate. Hence it will be our goal to minimize the integrated autocorrelation time, by taking into account only those configurations which are uncorrelated, i.e. where the autocorrelation time is equal to unity: $2\tau^{int} = 1$. In the simulation this is realized by skipping a certain number of trajectories, or configuration samples, before saving the next one, which should not be correlated to the previous one beeing saved.

Thus now in principle we are in the position to calculate the errors of the ensemble average over configurations. For the correlation function, where we have to calculate several ensemble averages, this would mean, that for each configuration we compute a correlator, after that the naive variance, which we devide by the number of samples. But actually, when we have derived the form the correlation function takes in the continnuum, we had to substract the vaccuum expectation value of the disconnected part. For the neutral pion this contribution takes the form $< 0|\pi(0)|0 >^2 = < \frac{1}{2}(Tr[G_u(0,0)] + Tr[G_d(0,0)]) >^2$. We will see that it is of the order of magnitude of the disconneted correlator. Hence we substract two correlated big numbers, to give a third small number. If we calculate the error of the difference by means of simple error propagation it will be unsignificantly big, as we would simply have to add the absolute errors.

In contrast to that we can compute the real statistical error by a method called the **jackknife** [11], which takes into account the statistical correlations of the terms we substract. Suppose for example that we want to compute the error for an estimator $\hat{\theta} = s(\mathbf{C})$ where we have a sample $\mathbf{C}$ of N configurations $\mathbf{C} = (C_1, C_2, C_3, ..., C_N)$. Then we define the jackknife samples:

$$\mathbf{C}_{(i)} = (C_1, C_2, C_3, ..., C_{i-1}, C_{i+1}, ..., C_N)\,, \tag{81}$$

where the i-th jackknife sample constists of the whole data set with configuration C_i removed. Accordingly we call $\hat{\theta}_i = s(\mathbf{C}_{(i)})$ the jackknife replicas of $\hat{\theta}$. After introducing the mean

$$\hat{\theta}_{(*)} = \sum_{i=1}^{N} \hat{\theta}_{(i)}/N \tag{82}$$

of jackknife replicas we finally find that the jackknife estimate of the standard error takes the form:

$$\hat{\sigma}_{jack} = \sqrt{\frac{N-1}{N} \sum_{i=1}^{N} (\hat{\theta}_{(i)} - \hat{\theta}_{(*)})^2}\,. \tag{83}$$

By considering the special case $\hat{\theta} = \bar{x}$ for the estimator, we observe that here the error of the mean value is:

$$\hat{\sigma}_{jack} = \sqrt{\frac{1}{N(N-1)} \sum_{i=1}^{N} (x_{(i)} - \bar{x})^2}\,, \tag{84}$$

because $\hat{\theta}_{(*)} = \bar{x}$ and $\hat{\theta}_{(i)} = \frac{N}{N-1}\bar{x} - \frac{x_{(i)}}{N-1}$.
This motivates the prefactor of $(N-1)/N$. We could of course also use the prefactor $[(N-1)/N]^2$ to obtain the usual standard error estimate for the mean given by:

$$\hat{\sigma}_{\bar{x}} = \sqrt{\frac{1}{N^2} \sum_{i=1}^{N} (x_{(i)} - \bar{x})^2}\,. \tag{85}$$

But the jackknife convention will for large N clearly coincide whith this choice yealding the standard error.

3.3 Use of stochastic sources

In the final part of this section we would like to discuss a last tool of great importance for the computation of the fermionic propagators. The naive way to calculate a fermion propagator is as follows. We have seen that the propagator extracted from the path integration of the fermionic Grassmann variables is nothing but the inverse of the Dirac operator:

$$\not{D}(x,y)^{-1} = G(x,y)\,. \tag{86}$$

So let us consider a spinor $\Psi_j(x)$ with space-time indices x and and spin and colour indices j, which after the action of the Dirac operator on it yields a δ-function:

$$\not{D}(x,y)_{jk}\Psi_j(x) = \delta_k(y) \tag{87}$$

δ-function here means that we have a matrix with one entry at position (x,k) only, which in the following we refer to as a point-source. By solving Equation (89) for $\Psi_j(x)$ we can obtain one column vector $\Psi_j(x)$ of the propagator matrix G called **one-to-all propagator**:

$$\Psi_j(x) = G_{jk}(x,y)\delta_k(y) \tag{88}$$

for each point source δ.
This equation can be solved by the conjugate gradient method for example. We invert one column of the Dirac operator matrix for each point source, which for all point sources gives us the complete propagator. Clearly, as the size of the matrix is growing with the square of the volume, the computational cost of this operation is increasing rapdidly on larger lattices. Thus we can try to employ fewer point sources and use the translational invariance of the correlator. But clearly this will suppress a large number of statistical information contained in the remaining volume part of the propagator depending on the configurations.

Hence another strategy has been proposed where we use so called **stochastic sources** [10]. These stochastic sources are designed to fulfill the Gaussian noise properties:

$$[\eta_{a\mu}(t,\vec{x})] = 0 \tag{89}$$

$$[\eta_{a\mu}(t,\vec{x})\eta_{b\nu}(\tau,\vec{y})] = \delta_{ab}\delta_{\mu\nu}\delta_{t\tau}\delta_{\vec{x}\vec{y}}\,, \tag{90}$$

when averaging over a large number of samples, which is denoted by the average [*]. From that it immediately follows that we can calculate the propagator by contracting a source and the inverse of a source given by:

$$\Psi_j(t,x) = G_{jk}(t,x,\tau,y)\eta_k(\tau,y)\,, \tag{91}$$

$$[\eta_i(t,\vec{x})\Psi_j(\tau,\vec{y})] = [\eta_i(t,x)G_{jk}(\tau,\vec{y},t',\vec{z})\eta_k(t',z)] = G_{ji}(\tau,\vec{y},t,\vec{x}) + noise\,. \tag{92}$$

Hence the terms in the disconnected part of the propagator can be calculated like follows:

$$Tr\sum_x G(t,\vec{x},t,\vec{x}) = \sum_x\sum_{a,\mu} G^{aa}_{\mu\mu}(t,\vec{x},t,\vec{x}) = \sum_{x,a,\mu}\sum_{y,b,\nu}\sum_{\tau} G^{ab}_{\mu\nu}(t,\vec{x},\tau,\vec{y})\delta_{ab}\delta_{\mu\nu}\delta_{\vec{x}\vec{y}}\delta_{t\tau} \tag{93}$$

$$= \sum_{x,a,\mu}\sum_{y,b,\nu}\sum_{\tau} G^{ab}_{\mu\nu}(t,\vec{x},\tau,\vec{y})[\eta_{a\mu}(t,\vec{x})\eta_{b\nu}(\tau,\vec{y})] = \sum_{x,a,\mu}[\eta_{a\mu}(t,\vec{x})\Psi_{a\mu}(t,\vec{x})] \tag{94}$$

Of course here we have introduced an additional error consisting in the stochastic noise. As we have introduced one stochastic source, we can assume it to be proportional to the volume.
So the variance for N_S stochastic sources (we count all sources, point and stochastic, per time-slice and spin-colour index) is of order $\sqrt{\frac{V}{N_S}}$ while the signal is at best of order unity.
When calculating the connected contribution of the correlator we can employ an even more favorable strategy called the **One-end-trick**:

$$[\psi_i(t,\vec{x})^+\psi_j(\tau,\vec{y})] = [(G^+_{ik}(t,\vec{x},t',\vec{x}')\eta^*_k(t',\vec{x}'))G_{jm}(\tau,\vec{y},\tau',\vec{y}')\eta_m(\tau',\vec{y}')] \tag{95}$$

$$= \sum_{t',\vec{x}',k} G^+_{ik}(t,\vec{x},t',\vec{x}')G_{jk}(\tau,\vec{y},t',\vec{x}') + noise\,. \tag{96}$$

Here we use two stochastic sources, which means that the variance of the noise is of order $\frac{V}{\sqrt{N_S}}$, but the signal now is of order V because of the contraction. In practice we have realized the stochastic sources as $\mathcal{Z}(2) = \pm 1$ wall sources. Each entry of the source is drawn from the distribution $\mathcal{Z}(2)$ over the whole space volume at a fixed time-slice and spin-colour component. An alternative approach would be to choose the distribution $\mathcal{Z}(2)\otimes\mathcal{Z}(2) = \frac{1}{\sqrt{2}}(\pm 1 \pm i)$. These propagators thus have the property to fill the whole volume and are called **all-to-all propagators**. Figure 3 shows that the stochastic noise scales very nicely as $\frac{Noise}{\sqrt{N_S}}$. I have plotted the jackknife error of the disconnected contribution at timeslice 0 times the squareroot of the number of the stochastic sources N_S against N_S for one fixed gauge field but up to $N_S = 100000$ sources on a $4^3 \times 8$ lattice.

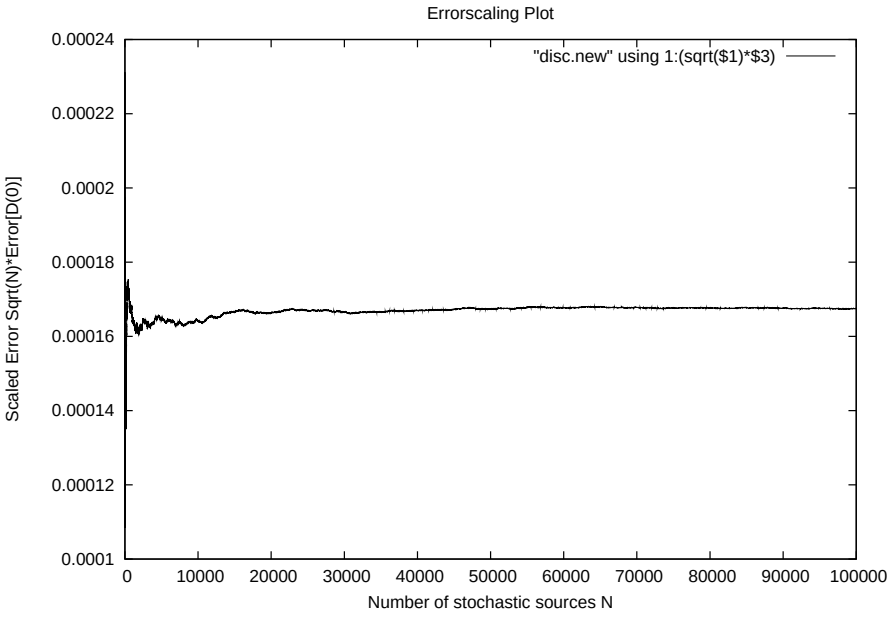

Figure 3: Errorscaling of the disconnected part of the π^0 correlator for one fixed gauge field in dependence of the number of stochastic sources

4 Error studies

In this section we discuss how to optimize the calculation of meson masses and correlation functions in terms of the error we obtain for a given computational cost.
One of the main aspects of my ongoing work was to investigate the error of the connected and disconnected contributions to the pion correlator, namely the scaling of this error with the number of stochastic sources and the number of gauge fields. I have therefore run the HMC-algorithm, created a certain number of up to 1000 configurations and inverted the Dirac operator for these configurations to obtain propagators of point and stochastic sources.
First of all I have found, that the error in the connected contributions to the pion correlator compared to the disconnected contributions is so small, that it is possible to calculate the $\pi^{\pm}$ or connected correlator using point sources at a fixed timeslice and volume point only instead of stochastic sources.
It is important to note that it is not advantageous to invert point sources at all space time points as is shown in the table below. We have tried to do so and compared the two correlators we have obtained for 10 gauge fields:

Timeslice	$\pi^{\pm}$ Correlator at fixed volume point	Error in 10 gauge fields	$\pi^{\pm}$ Correlator for all point sources	Error in 10 gauge fields
0	1.28337	0.00319	1.28230	0.000714
1	0.144515	0.001041	0.143443	0.0003542
2	0.0135875	0.0003457	0.0138218	0.0000669
3	0.00140426	0.00005038	0.00146531	0.00001121
4	0.000306584	0.00001084	0.000312552	0.00000426

Hence by increasing the inversions by a factor $L \times L \times L \times T$ we improve the error by a factor of 4 only. This could also have been achieved by taking 16 times the number of gauge fields and hence increasing the number of inversions by a factor of only 16, where we assume that the error scales as expected in the number of gauge fields. This we will see later.

In practice this strategy is necessary too, because considering the available disk space it is not possible to store or create point one-to-all propagators for hundreds of gauge fields times with a space-time volume of the order of $24^3 \times 48$ (which is a typical lattice size).

We have also used a number of 10 and 25 stochastic volume sources for 10 gauge fields, which is shown in the table below. We can see that using the One-end-trick [Section 3.3] we obtain an error as big as for all one-to-all propagators:

Timeslice	$\pi^{\pm}$ Correlator for 10 stochastic sources (Error)	$\pi^{\pm}$ Correlator for 25 stochastic sources (Error)
0	1.2831(9)	1.2822(9)
1	0.1433(4)	0.1433(4)

We can hence decrease the number of inversions that we need, by a factor of $\frac{L \times L \times L}{10}$ since there is no improvement in the error for 25 compared to 10 stochastic sources.

Now when calculating the π^0 correlator we will need to consider the disconnected quark diagrams as well. Figure 4 shows, on the right side, that the error in the disconnected part is much smaller, compared to the connected contribution at timeslice 1 on this $8^3 \times 16$ lattice. On the other hand the relative error is much bigger for the disconnected pieces and is falling off much slower as is shown on the left side. This means, that the error of the disconnected contribution gets dominant at larger timeslices [also see Figure 9 later], because there the disconnected part is dominating the correlation function. Hence to achieve a higher efficiency it is of advantage to use stochastic all-to-all propagators instead of point sources. For example consider a $4^3 \times 8$ lattice. Here we would need $4^3 \times 8 = 512$ one-to-all propagators . As the main computational cost comes from the inversions, this is as expensive as 512 stochastic sources.

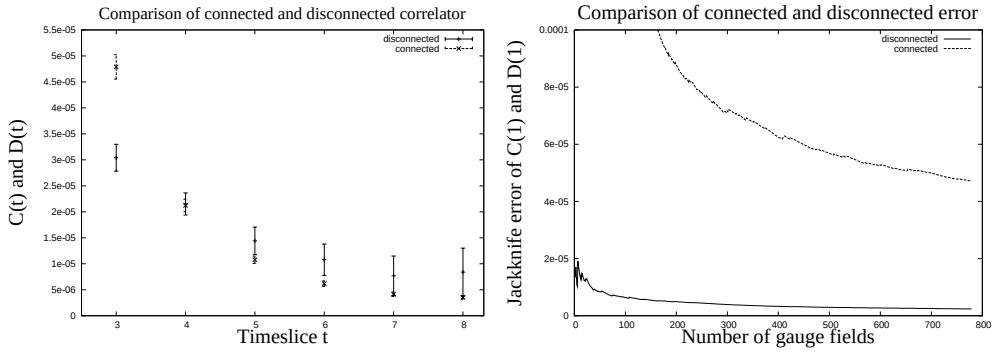

Figure 4: Comparison of the connected and disconnected contributions and comparison of their errors

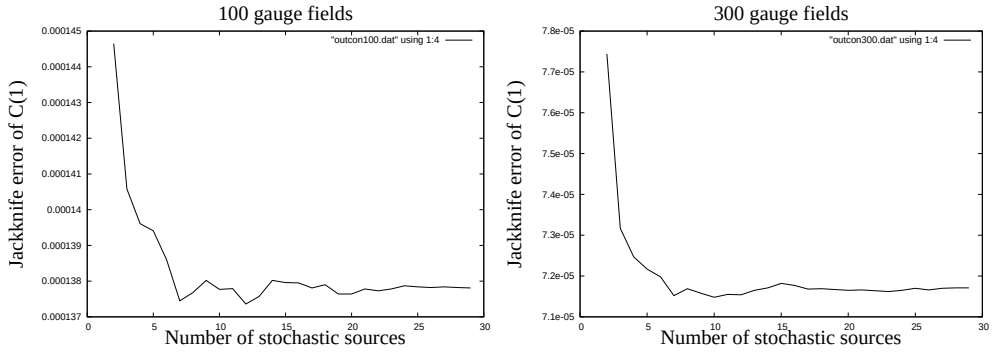

Figure 5: Error of the π^0 correlator averaged over a fixed number of gauge fields depending on N_S

In Figure 5 we have plotted the error of the pion correlator at timeslice 1 against the number of stochastic sources using 100 gauge fields in the left part. The simulation has been performed on a $4^3 \times 8$ lattice. One can see from the plateau in Figure 5 that the stochastic noise becomes negligible for a number of ten stochastic sources and is dominated by the statistical gauge field fluctuations. Thus we can use 10 stochastic sources instead of 512 point sources, a ratio which becomes better and better for larger lattices.
Hence we have found that only $\mathcal{O}(10)$ inversions are necessary per gauge field.
Moreover we can see in Figures 6 and 7, that beyond this number of $N_S = 10$ stochastic sources (here we choose 12 and 25) the error scales very smoothly in the number of gauge fields. In Figure 6 we show the error of the disconnected contribution at timeslice 1 depending on the number of gauge fields for a fixed number of 12 and 25 stochastic sources. In Figure 7 we have plotted the error of the π^0 correlator at timeslice 1 times $\sqrt{N_G}$, i.e. $C(1) \times \sqrt{N_G}$ against N_G the number of gauge fields. We have done this for 12 stochastic sources in the left part, and for 25 stochastic sources on the right hand side.

Our stratey thus is to calculate the connected part using point sources at a fixed volume point.
We compute the noisy disconnected part using a number of $\mathcal{O}(10)$ stochastic sources to achieve a resulting error which is of the order of magnitude of the connected $\pi^{\pm}$ correlator contribution.
Then the stochastic noise will be suppressed and the error scales as expected in the number of gauge fields.

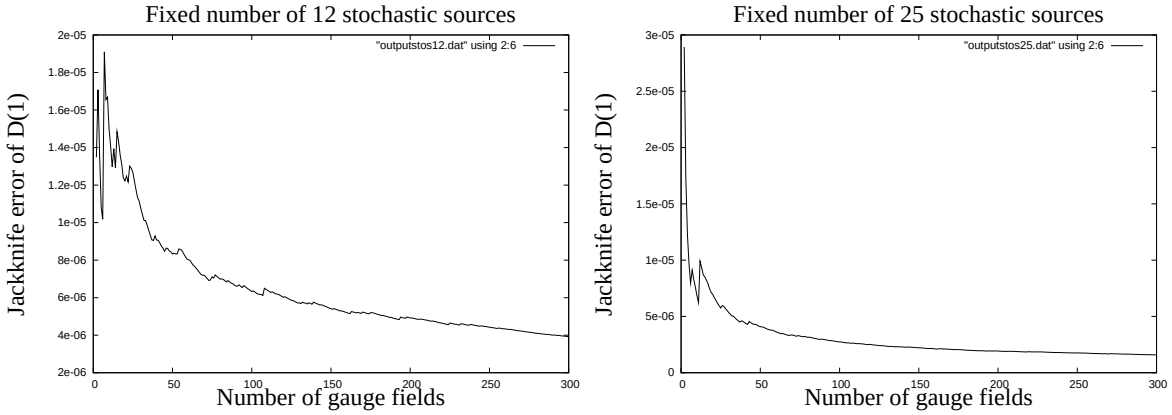

Figure 6: Error of the disconnected part of the π^0 correlator for a fixed number of stochastic sources in dependence of the number of gauge fields

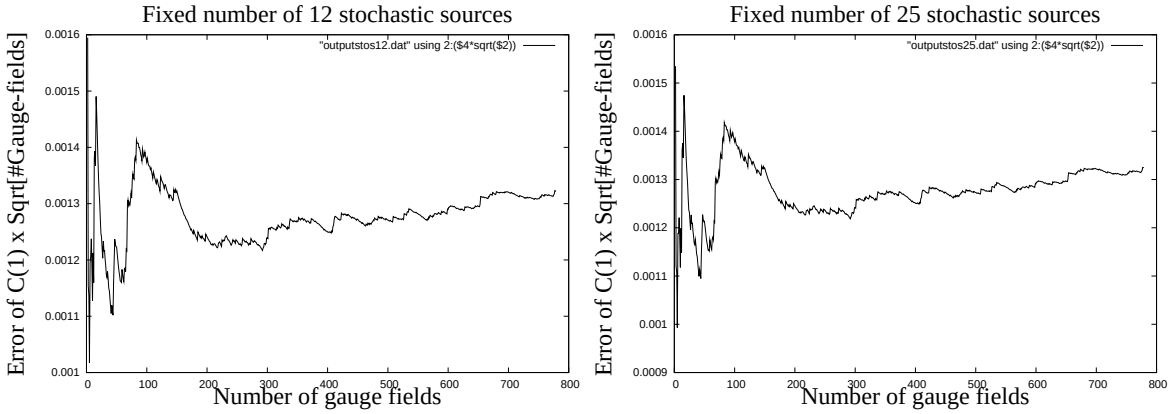

Figure 7: Error of the π^0 correlator for a fixed number of stochastic sources in dependence of the number of gauge fields

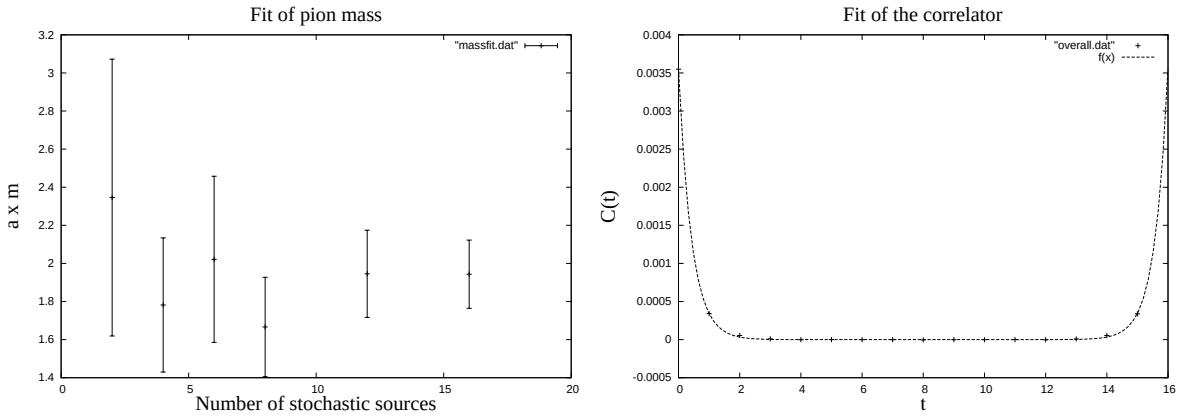

Figure 8: Pion masses fitted from the π^0 correlator for a fixed number of gauge fields in dependence of the number of stochastic sources on a $8^3 \times 16$ lattice

5 Final results

In Figure 8 we illustrate how our result for the pion mass for a lattice spacing of a=0.08 fm is affected by the noise arising from the stochastic sources. We have fitted the correlator arising from connected and disconnected contributions to a pion mass. This is shown in the right image, where we have plotted the data points that we have obtained for the correlator with errorbars and that we have fitted with a function $f(x) = A * \cosh(am(x - \frac{T}{2}))$.
We obtain pion masses in lattice units $a \times m$ for a number of 2 to 16 stochastic sources. The simulation has been performed on a $8^3 \times 16$ lattice. In the left image one can clearly see, that the error in the pion mass is decreasing with the number of stochastic sources. Moreover there is no significant change in the error for a number of more then 10 stochastic sources. On the right hand side we show the fit of the correlation function. Hence we have confirmed that this is a reasonable number of stochastic sources to work with.

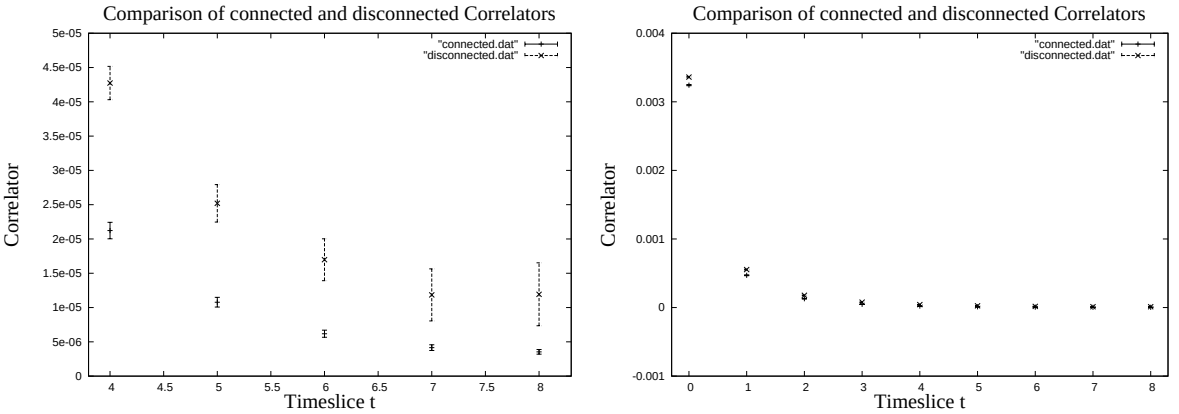

Figure 9: Comparison of the $\pi^{\pm}$ and π^0 correlators with errorbars in two different timeslice regions

Therefore we can plot the correlators of the $\pi^{\pm}$ and π^0 mesons with errorbars in Figure 9. We can clearly see on the left hand side, that the error of the disconnected part is dominating the error of the connected contribution at larger timeslices, where it is also dominating the correlator. This also justifies that we take selected point sources for the connected contribution and stochastic sources for the disconnected part, because the stochastic sources are only necessary to increase the efficiency for the disconnected part, which has a big relative error. This relative error is dominating the overall relative error.

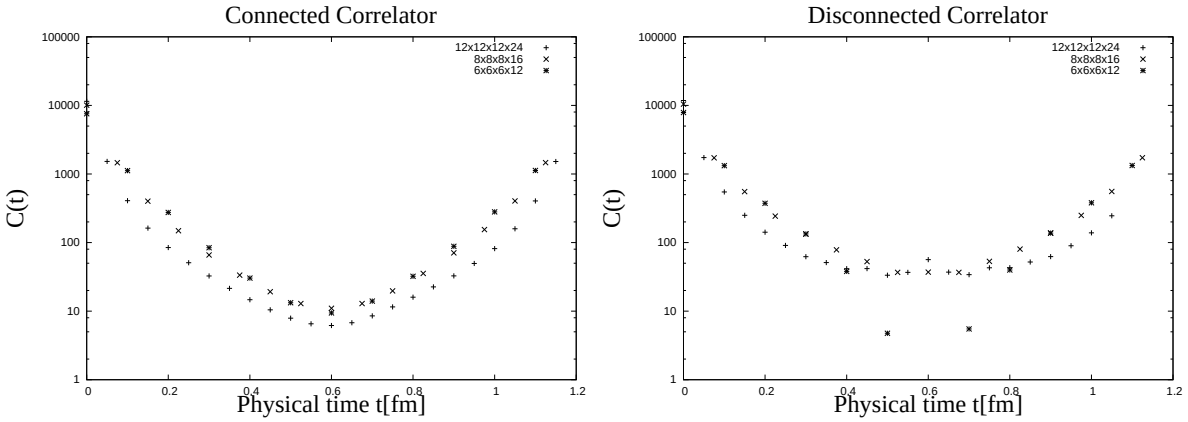

Figure 10: Plot of the scaled $\pi^{\pm}$ and π^0 correlators with errorbars

Finally we have computed the disconnected and connected correlators at lattice spacings of a=0.1 fm on a $6^3 \times 12$ lattice, at a=0.08 fm on a $8^3 \times 16$ lattice and at a=0.065 fm on a $12^3 \times 24$ lattice. We have scaled these correlators of dimension 6 according to the lattice spacing and plotted them against physical time $t_{phys} = t \times a$ in Figure 10. Unfortunately there is a slight mismatch in the volume of the lattice. This mismatch is the biggest for the large $12^3 \times 24$ lattice, so that the corresponding correlator is clearly differing from the other two, as you can see in the left part of Figure 10, where we have plotted the $\pi^{\pm}$ correlators. In principle, at equal volume, these correlators should coincide, as our parameters are tuned to keep the $\pi^{\pm}$ mass constant for each lattice spacing and we are working at maximal twist such that the lattice spacing artefacts should be very small.

We compare the averaged sum of the scaled correlators in the following table.

Lattice	Physical L [fm]	a [fm]	$\pi^{\pm}$ Correlator $\frac{1}{T}\sum_t C(t)$	π^0 Correlator $\frac{1}{T}\sum_t$[C(t)+D(t)]
$6^3 \times 12$	0.61	0.1	886(5)	969(12)
$8^3 \times 16$	0.66	0.082	899(9)	1009(15)
$12^3 \times 24$	0.79	0.065	672(4)	745(10)

Again it can be seen that for the almost matched lattices ($6^3 \times 12$ at a=0.1 fm and $8^3 \times 16$ at a = 0.08 fm) a nice scaling in the lattice spacing is observed while for the unmatched lattice ($12^3 \times 24$ at a=0.0065 fm) a clear discrepancy is observed. Moreover, there is also a significant difference between the $\pi^{\pm}$ and the π^0 correlators indicating the inherent parity violation of twisted-mass fermions at non-zero lattice spacings. In this report, we could not demonstrate, that this lattice artefact vanishes in the continuum limit and this question will be the subject of my further work.

We have also plotted the π^0 correlator in the right part of Figure 10. Here you can see the same effect. We also identify big errorbars in the middle of the plot, arising from the disconnected contributions. As we could use only 3 stochastic sources for the big lattice we can see that on a big lattice this is already sufficient, while with 10 stochastic sources on the small lattice we still obtain unsignificant values for the disconnected contribution at large timeslices. Hence we again can state, that this part of the correlator is noisy.
In principle, at equal volume, one should also be able to show $\mathcal{O}$(a) improvement for these lattice spacings, which means that the π^0 mass is depending linear on a^2 at small lattice spacings.

The pion mass is in general extracted by first of all plotting the effective mass,

$$m_{eff}(t+\frac{1}{2}) = -\ln\frac{C(t+1)}{C(t)}\,, \tag{97}$$

against time. As we have seen in Section 2.3 only in the limit $t \to \infty$ excited states will be removed. However in the middle of the lattice at $t = \frac{T}{2}$ we will clearly see finite size effects just arising from our boundary conditions, which lead to the overlap of exponentials e^{-mat} and $e^{-ma(T-t)}$ yielding a $\cosh(ma(t-\frac{T}{2}))$ function. But, we here are only fitting to an exponential. Hence we are looking for a plateau, where the effects arising from finite size and the excited states are still negligible. We have obtained such a plateau on a $12^3 \times 24$ lattice. It is shown in Figure 11, where we plot the effective mass $m_{eff}(t+\frac{1}{2})$ depending on the timeslice t.

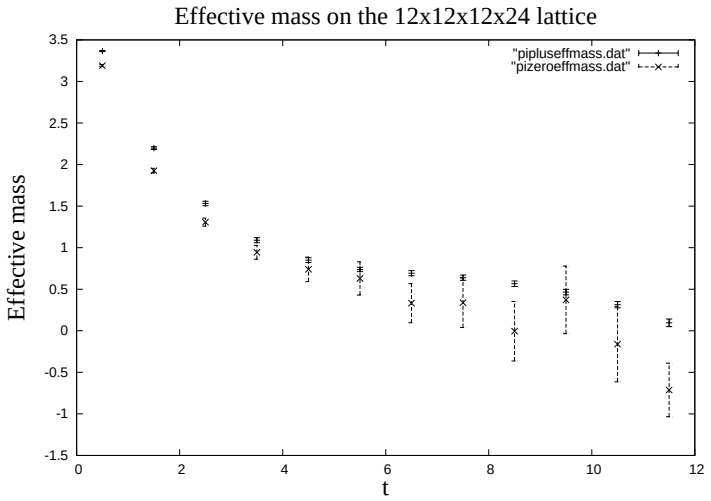

Figure 11: Plot of m_{eff} for the $\pi^{\pm}$ and π^0 correlators with errorbars

One can clearly see that the errorbars of the overall π^0 correlator are dominated by the disconnected contributions, as they are much bigger than the errorbars of the connected $\pi^{\pm}$ part. We also identify the $\pi^{\pm}$ mass to be bigger than the π^0 mass, in consistency with results of ref. [5].

6 Conclusions

This project first of all has enlightened my understanding of lattice QCD as a whole, regarding theoretical foundations and practical methods.
During the period at DESY Zeuthen, I have thus learned how to use methods for the reduction of errors in the calculation of correlation functions. I have also gained a comprehension on how to extract physical masses from these correlation functions. Now I am able to employ stochastic methods to investigate disconnected quark diagrams, which are important for the computation of the $\eta\prime$ mass in particular. Also I am now familiar with existing code and packages, in view of a further investigation of the $\eta\prime$ mass. I have seen that twisted-mass QCD breaks flavour symmetry leading to a difference in the $\pi^{\pm}$ and π^0 mass. It remains to show that this difference is vanishing with $\mathcal{O}(a^2)$, as flavour symmetry is restored in the continuum limit, and because of automatic $\mathcal{O}$(a) improvement in maximally twisted-mass QCD. This will be the task for the following weeks to come. At the same time it will be possible to extract the physical mass of the three pions by taking the continuum limit.
However I can conclude that the computation of meson masses from first principles is by now well understood for the case of the pion triplet, comprising, in particular, the calculation of the connected and disconnected contributions. Thus I am able to proceed now to the calculation of other mesons as well, with a particular focus of the $\eta\prime$ mass.

A Monte-Carlo methods

In this Appendix we briefly discuss methods for the evaluation of path integrals over gauge field configurations. If we want to calculate the expectation value of an observable numerically, one standard way is the Monte-Carlo method. The idea behind is to draw gauge field configurations, denoted by ϕ, distributed according to our Boltzmann factor $e^{-S[\phi]}$ with a probability distribution,

$$P(\phi_k)\mathcal{D}\phi = \frac{e^{-S[\phi]}\mathcal{D}\phi}{\int \mathcal{D}\phi e^{-S[\phi]}}\,. \tag{98}$$

In the literature this is refered to as **Importance Sampling**. Once we can generate sequences of configurations $(\phi_k)_{k\epsilon N}$ fulfilling this probability distribution, the expectation value of our observable O, turns out to be as simple as a sum,

$$\langle O\rangle = \frac{1}{N}\sum_{k=1}^{N} O(\phi_k)\,. \tag{99}$$

In the limit $N \to \infty$ this gives the value of O.

A.1 Markov chains

In order to realize importance sampling it is possible to use a Markov process to generate the N configurations ϕ_k. The elements W_{ij} of a Markov chain are called Markov steps and represent the probability that a system makes a transition $i \to j$. In the continnuum these steps (for transitions $\phi \to \phi'$) satisfy the following conditions.

$$W(\phi,\phi') \geq 0 \tag{100}$$

$$\int \mathcal{D}\phi' W(\phi,\phi') = 1 \tag{101}$$

We define the n-step process by,

$$W^{(n)}(\phi,\phi') = \int \mathcal{D}\phi_1 ... \int \mathcal{D}\phi_{n-1} W(\phi,\phi_1)W(\phi_1,\phi_2)...W(\phi_{n-1},\phi')\,. \tag{102}$$

One can show that in the long time behaviour a Markov process reaches equilibrium:

$$\lim_{n\to\infty} W^{(n)}(\phi,\phi') = P^{eq}(\phi')\,. \tag{103}$$

This is invariant under further Markov steps and thus an eigenvector of the Markov process. It is possible to show that P^{eq} is a probability distribution. Now in order to construct such a Markov process we need to fulfill the follwing conditions.

$$W(\phi,\phi') > 0 \tag{104}$$

$$\int \mathcal{D}\phi' W(\phi,\phi') = 1 \tag{105}$$

$$P^{eq}(\phi') = \int \mathcal{D}\phi P^{eq}(\phi) W(\phi,\phi') \tag{106}$$

This can be done by imposing the detailed balance condition:

$$\frac{W(\phi,\phi')}{W(\phi',\phi)} = \frac{P^{eq}(\phi')}{P^{eq}(\phi)}\,. \tag{107}$$

One way to satisfy the detailed balance condition is to choose

$$W(\phi,\phi') \sim e^{-S[\phi']}\,. \tag{108}$$

This method is called the **Heat Bath** algorithm.
In contrast in the **Metropolis** method one generates a random number R in the interval [0,1] and accepts the new configuration ϕ' only if $R \leq \frac{e^{-S[\phi']}}{e^{-S[\phi]}}$. Else the configuration is rejected and ϕ is kept. One can show that this algorithm satisfies detailed balance.

A.2 HMC algorithm

Note that in Statistical Mechanics there are well known methods to achieve such probability distributions. One of these methods is called the Hybrid-Monte-Carlo algorithm (HMC).
Let us try to obtain the HMC in a heuristic way. Our starting point is a stochastic differential equation, the Langevin equation (a famous description for Brownian motion),

$$\dot{\pi} = -\gamma\pi + \eta(t) \tag{109}$$

with π beeing the momentum of a particle driven by a random force η with the Gaussian noise properties $\langle\eta(t)\rangle = 0$ and $\langle\eta(t)\eta(t')\rangle = \delta(t-t')$ and γ is a friction coefficient.
The probability to find a particle with momentum π at a time t of this model is given by the Fokker-Planck equation:

$$\frac{\partial}{\partial t}P(\pi,t) = \gamma\frac{\partial}{\partial\pi}(\pi P) + \frac{1}{2}\frac{\partial^2 P}{\partial\pi^2}\,. \tag{110}$$

Moreover if we consider Brownian motion in an externel field $F = -\frac{\partial}{\partial\phi}V(\phi)$ we are lead to the following equations:

$$\dot{\phi} = \pi \tag{111}$$

$$\dot{\pi} = -\gamma\pi + F + \eta(t)\,. \tag{112}$$

This system of stochastic differential equations is equivalent to a generalized Fokker-Planck equation, the Kramers equation:

$$\frac{\partial}{\partial t}P(\phi,\pi,t) + \pi\frac{\partial P}{\partial\phi} + F(\phi)\frac{\partial P}{\partial\pi} = \gamma\frac{\partial}{\partial\pi}(\pi P) + \frac{1}{2}\frac{\partial^2 P}{\partial\pi^2}\,. \tag{113}$$

The solution of the Kramers equation in the limit of large time scales leads to the desired exponential probability distribution:

$$\lim_{t\to\infty} P(\phi,\pi,t) \propto e^{-\frac{\gamma}{2}\pi^2}e^{-V(\phi)}\,, \tag{114}$$

which we may compare to the expectation value of our operator:

$$\langle O\rangle = \frac{\int\mathcal{D}\phi O(\phi)e^{-S[\phi]}}{\int\mathcal{D}\phi e^{-S[\phi]}} = \frac{\int\mathcal{D}\phi\int\mathcal{D}\pi O(\phi)e^{-\frac{1}{2}\pi^2-S[\phi]}}{\int\mathcal{D}\phi\int\mathcal{D}\pi e^{-\frac{1}{2}\pi^2-S[\phi]}}\,, \tag{115}$$

where we have just added Gaussian integral factor of one and set $\gamma = 1$.
Thus we may consider a Hamiltonian:

$$H = \frac{1}{2}\pi^2 + S[\phi]\,. \tag{116}$$

This Hamiltonian depends on virtual momenta $\pi(\tau)$, which are Gaussian distributed in a virtual Monte-Carlo time τ:

$$\langle\pi(\tau)\rangle = 0 \tag{117}$$

$$\langle\pi(\tau)\pi(\tau')\rangle = \delta(\tau-\tau')\,. \tag{118}$$

Let us now evolve the system in the virtual Monte-Carlo time according to the set of stochastic differential equations

$$\dot{\phi} = \pi \tag{119}$$

$$\dot{\pi} = -\frac{\partial}{\partial\phi}S\,, \tag{120}$$

which we will refer to as Hamilton's equations. In analogy to the case of the Kramer's equations, in this virtual Monte-Carlo time our probability distribution converges to the desired form, namely the Boltzmann factor $e^{-S[\phi]}$. Thus our ingredients for the algorithm are the solutions of Hamilton's equations and to generate π as Gaussian distributed random number. After this, we are sure that we obtain the desired probability distribution for the final positions and momenta.

Numerically we may solve Hamilton's equations in a discretized form, using the so called leap-frog scheme (where we use alternating time steps of $\frac{\delta\tau}{2}$ for positions and momenta), which is time-invariant and cancels some of the discretization errors in $\delta\tau$, which denotes the non-zero step size in the numerical integration. In a first step we create the starting values at $\tau = 0$, which are a Gaussian distributed random number for $\pi(t)[0]$ and a flat random distribution for $\phi(t)[0]$. The second step is the integration of the Langevin equation via the leap-frog scheme

$$\pi(t)[\frac{\delta\tau}{2}] = \pi(t)[0] - \frac{\delta\tau}{2}[\frac{\partial}{\partial\phi}S]_{\phi[0]} \tag{121}$$

$$\phi(t)[\delta\tau] = \phi(t)[0] + \pi(t)[\frac{\delta\tau}{2}]\delta\tau \tag{122}$$

$$\pi(t)[3\frac{\delta\tau}{2}] = \pi(t)[\frac{\delta\tau}{2}] - \delta\tau[\frac{\partial}{\partial\phi}S]_{\phi[\delta\tau]} \tag{123}$$

etc. Moreover, in a third step, we can compensate for the discretization error by inserting a Metropolis like accept/reject step, i.e. we accept the new field configuration $[\phi_{end}, \pi_{end}]$ only as one of the "random numbers" with the acceptance probability:

$$P_{accept} = \min(1, e^{H(\phi_{in},\pi_{in})-H(\phi_{end},\pi_{end})}) . \tag{124}$$

This acceptance probabilty is realized by creating a random number $R\epsilon(0, 1]$: if $e^{\Delta H} < R$ then we accept, otherwise we do not. We create the next random values, by starting with the preceeding random value, which we put into the discretized Langevin equations and so on, until we have created the desired number of the random distributed $[\phi_k, \pi_k]$.

B Gauge fields on the lattice

B.1 Abelian gauge fields on the lattice

All physical quantities are gauge invariant. Hence we are in a need to formulate a gauge invariant lattice action. In section 2.1 we have considered the continuum action of the free Dirac field:

$$S_F[\Psi, \bar{\Psi}] = \int d^4x \bar{\Psi}(x)(i\gamma^\mu\partial_\mu + M)\Psi(x) . \tag{125}$$

If we consider this action to be invariant under local U(1) gauge transformations,

$$\Psi(x) \to G(x)\Psi(x) \tag{126}$$

$$\bar{\Psi}(x) \to \bar{\Psi}(x)G^{-1}(x) , \tag{127}$$

where the element of the group U(1) is given by

$$G(x) = e^{i\Lambda(x)} , \tag{128}$$

then we have to replace the partial derivative by the covariant derivative,

$$D_\mu = \partial_\mu + ieA_\mu , \tag{129}$$

resulting in the Euclidean action of QED,

$$S_{QED}[\Psi, \bar{\Psi}] = -\frac{1}{4}\int d^4x F^{\mu\nu}(x)F_{\mu\nu}(x) + \int d^4x \bar{\Psi}(x)(i\gamma^\mu D_\mu + M)\Psi(x) , \tag{130}$$

where we have added the kinetic term for the gauge field. In section 2.1 we have seen a discretization of the free fermionic action, where terms of the following form appear:

$$\bar{\Psi}(x)\Psi(y) \to \bar{\Psi}(x)G^{-1}(x)G(y)\Psi(y) . \tag{131}$$

To make these gauge invariant we consider the **Schwinger line integral**:

$$U(x,y) = e^{ie\int_x^y dz_\mu A_\mu(z)} \to G(x)U(x,y)^{-1}(y)\,, \tag{132}$$

under the gauge transformation:

$$A_\mu \to A_\mu - \frac{1}{e}\partial_\mu \Lambda\,. \tag{133}$$

Accordingly we identify $\bar{\Psi}(x)U(x,y)\Psi(y)$ to be gauge invariant. Thus in discretized form we modify the terms like,

$$\bar{\Psi}(x)\Psi(x+\hat{\mu}) \to \bar{\Psi}(x)U(x,x+\hat{\mu})\Psi(x+\hat{\mu}) \tag{134}$$

$$\bar{\Psi}(x+\hat{\mu})\Psi(x) \to \bar{\Psi}(x+\hat{\mu})U(x+\hat{\mu},x)\Psi(x) \tag{135}$$

with the gauge field **link** at lattice spacing a:

$$U(x,x+\hat{\mu}) = e^{ieaA_\mu(x)}\,. \tag{136}$$

We conclude that the U(1) gauge invariant action for Wilson type fermions is:

$$S_F^{(W)}[\Psi,\bar{\Psi},U] = (\hat{M}+4r)\sum_n \bar{\Psi}(n)\Psi(n) \tag{137}$$

$$-\frac{1}{2}\sum_{n,\mu}[\bar{\Psi}(n)(r-\gamma_\mu)U(n,n+\hat{\mu})\Psi(n+\hat{\mu}) + \bar{\Psi}(n+\hat{\mu})(r+\gamma_\mu)U^+(n,n+\hat{\mu})\Psi(n)]\,. \tag{138}$$

B.2 Gauge field action and the Wilson loop

In this section we define the plaquette,

$$U_{\mu\nu}(x) = U(x,x+\hat{\mu})U(x+\hat{\mu},x+\hat{\mu}+\hat{\nu})U^+(x+\hat{\nu},x+\hat{\nu}+\hat{\mu})U^+(x,x+\hat{\nu})\,, \tag{139}$$

which with the discretized form of the field strength tensor

$$F_{\mu\nu}(x) = \frac{1}{a}[(A_\nu(x+\hat{\mu}) - A_\nu(x)) - (A_\mu(x+\hat{\nu}) - A_\mu(x))] \tag{140}$$

results in

$$U_{\mu\nu}(x) = e^{iea^2F_{\mu\nu}(x)} \simeq 1 + iea^2F_{\mu\nu}(x) - e^2a^4F_{\mu\nu}(x)F_{\mu\nu}(x) \tag{141}$$

at small lattice spacings. We can identify this plaquette to be the discretized verion of the **Wilson loop** [4],

$$U_P(x,x) = e^{ie\oint_P dz^\mu A_\mu(z)}\,, \tag{142}$$

where P is a closed path from x to x. Hence the gauge field action can be expressed as:

$$S_G[U] = -\frac{1}{4}\int d^4x F^{\mu\nu}(x)F_{\mu\nu}(x) \tag{143}$$

$$\simeq \sum_{x,\mu,\nu} a^4 F_{\mu\nu}(x)F_{\mu\nu}(x) \tag{144}$$

$$\Rightarrow S_G[U] \simeq \frac{1}{e^2}\sum_x\sum_{\mu<\nu}[1 - \frac{1}{2}(U_{\mu\nu}(x) + U^+_{\mu\nu}(x))]\,. \tag{145}$$

B.3 Non-Abelian gauge fields on the lattice

Let us now generalize the case of the U(1) gauge symmetry to the case of the non-Abelian unitary group SU(N). Therefore we introduce N-component spinor fields,

$$\vec{\Psi} = \begin{pmatrix} \Psi^1 \\ \Psi^2 \\ \Psi^3 \\ . \\ . \\ . \\ \Psi^N \end{pmatrix} , \vec{\bar{\Psi}} = \left(\bar{\Psi}^1, \quad \bar{\Psi}^2, \quad \bar{\Psi}^3, \quad . \quad . \quad . \quad , \bar{\Psi}^N\right) \tag{146}$$

transforming in analogy to the Abelian case as,

$$\vec{\Psi}(x) \to G(x)\vec{\Psi}(x) \tag{147}$$

$$\vec{\bar{\Psi}}(x) \to \vec{\bar{\Psi}}(x)G^{-1}(x) \tag{148}$$

$$\tag{149}$$

where now G(x) is an element of the fundamental representation of the group SU(N).
Then the link variables are simply replaced by matrices in colour space:

$$U(x, x+\hat{\mu}) = e^{ig_0 a A_\mu(x)} . \tag{150}$$

With these replacements we retain the same form of the action for Wilson fermions. However as the gauge field action in the continuum, which is

$$S_G = \frac{1}{2} Tr \int d^4x F_{\mu\nu} F_{\mu\nu} = \frac{1}{4} \int d^4x F^B_{\mu\nu} F^B_{\mu\nu} , \tag{151}$$

now contains a trace over the matrix valued field strength, we also obtain obtain a matrix for the case of the Wilson plaquette.

$$U_{\mu\nu}(x) = e^{ig_0 a^2 F_{\mu\nu}(x)} \tag{152}$$

One can explicitly show that also in matrix representation

$$S_G = \frac{2}{g_0^2} Tr \sum_x \sum_{\mu<\nu} [1 - \frac{1}{2}(U_{\mu\nu}(x) + U^+_{\mu\nu}(x))] \tag{153}$$

again gives the right continuum limit.

C O(a) improvement

In this Appendix we briefly mention techniques to improve the Lattice action so that $\mathcal{O}(a)$ cutoff-effects are suppressed, which is automatically the case for the Wilson twisted-mass fermions. The approach of Symanzik is to consider the unimproved lattice action

$$S[\bar{\chi},\chi,U] = S_G[U] + S_F[\bar{\chi},\chi,U] \tag{154}$$

as a local effective theory close to the continuum limit, neglecting small distance properties:

$$S_{eff} = S_0 + aS_1 + a^2 S_2 + \dots . \tag{155}$$

Since we are interested only in $\mathcal{O}(a)$ effects here we neglect the quadratic order gauge field lattice action. Thus for the Wilson twisted-mass fermions we find to leading order the renormalized continuum action:

$$S_0 = \int d^4x \bar{\chi}(x)[\gamma_\mu D_\mu + m_R + i\mu_R\gamma_5\tau^3]\chi(x)\,. \tag{156}$$

The improvement program would now consist in adding counterterms to the next to leading order term S_1 leading to an $\mathcal{O}(a)$ improved, so called clover action $S_{impr}[\bar{\chi},\chi,U] = S[\bar{\chi},\chi,U] + \delta S[\bar{\chi},\chi,U]$.
Let us now have a look at automatic $\mathcal{O}(a)$ improvement at maximal twist, $m_q = 0$: One can show that $\mathcal{R}_5^{1,2} \times \tilde{\mathcal{D}}$ is a symmetry of the lattice action $\int d^4x \bar{\chi}(x)[\gamma_\mu D_\mu + +i\mu_R\gamma_5\tau^3]\chi(x)$ where,

$$\mathcal{R}_5^{1,2} = \begin{cases} \chi(x_0,\vec{x}) \to i\gamma_5\tau^{1,2}\chi(x_0,\vec{x}) \\ \bar{\chi}(x_0,\vec{x}) \to \bar{\chi}(x_0,\vec{x})i\gamma_5\tau^{1,2} \end{cases}$$

is the discrete chiral symmetry corresponding to the two doublet components, often refered to as $\mathcal{R}_5$**-parity**, and $\tilde{\mathcal{D}} = \mathcal{D} \times [\mu_q \to -\mu_q]$ counts the dimensions of the operators including the mass given that:

$$\mathcal{D} = \begin{cases} U(x,\mu) \to U^+(-x - a\hat{\mu};\mu) \\ \chi(x) \to e^{3i\pi/2}\chi(-x) \\ \bar{\chi}(x) \to \bar{\chi}(-x)e^{3i\pi/2}\,. \end{cases}$$

If we now consider a lattice correlation function of the field ϕ, which in the effective theory is represented by an effective field $\phi_{eff} = \phi_0 + a\phi_1 + ...$ the lattice correlation function of this field up to $\mathcal{O}$(a) can be written as,

$$< \phi_0 > = < \phi_0 >_0 - a\int d^4y < \phi_0\mathcal{L}_1(y) >_0 + a < \phi_1 >_0 + \mathcal{O}(a^2)\,, \tag{157}$$

where we have introduced the next to leading order Lagrangian given by $S_1 = \int d^4y\mathcal{L}_1(y)$. Then one has claimed that because $\mathcal{R}_5^{1,2} \times \tilde{\mathcal{D}}$ is an exact symmetry of the system all $\mathcal{O}(a)$ terms must vanish, since one can check that all possible terms contributing to $\mathcal{L}_1$ are odd under this symmetry and ϕ_1 has opposite chirality compared to ϕ_0, as it is of one dimension higher, while the action is chirality invariant. Hence the correlation function is $\mathcal{O}(a)$ improved [8,12].

D Pion operators in twisted basis

In this Appendix we illustrate the transformation from the physical to the twisted basis by means of the example of the neutral pion. Consider the general chiral transformations,

$$u_{phys} = e^{-i\gamma_5\omega/2}u \tag{158}$$

$$\bar{u}_{phys} = \bar{u}e^{-i\gamma_5\omega/2} \tag{159}$$

$$d_{phys} = e^{i\gamma_5\omega/2}d \tag{160}$$

$$\bar{d}_{phys} = \bar{d}e^{i\gamma_5\omega/2}\,. \tag{161}$$

These can be expressed in terms of a scalar and a pseudoscalar term,

$$u_{phys} = e^{-i\gamma_5\omega\pi/2}u = [cos(\omega/2) - i\gamma_5 sin(\omega/2)]u \tag{162}$$

$$d_{phys} = e^{i\gamma_5\omega\pi/2}d = [cos(\omega/2) + i\gamma_5 sin(\omega/2)]d\,, \tag{163}$$

because

$$e^{i\gamma_5\omega/2} = cos(\omega/2) + i\gamma_5 sin(\omega/2)\,. \tag{164}$$

The field operator of the neutral pion, which physically is pseudoscalar reads:

$$\pi^0 = i\frac{1}{\sqrt{2}}(\bar{u}_{phys}\gamma_5 u_{phys} + \bar{d}_{phys}\gamma_5 d_{phys})\,. \tag{165}$$

Hence under the chiral transformations this becomes,

$$\pi^0 = \frac{i}{\sqrt{2}}((cos(\omega/2) - i\gamma_5 sin(\omega/2))\bar{u}\gamma_5 u(cos(\omega/2) - i\gamma_5 sin(\omega/2)) \tag{166}$$

$$+(cos(\omega/2) + i\gamma_5 sin(\omega/2))\bar{d}\gamma_5 d(cos(\omega/2) + i\gamma_5 sin(\omega/2))) \tag{167}$$

$$= \frac{1}{\sqrt{2}}[i(cos^2(\omega/2) - sin^2(\omega/2))(\bar{u}\gamma_5 u + \bar{d}\gamma_5 d) + 2sin(\omega/2)cos(\omega/2)(\bar{u}u + \bar{d}d)] \tag{168}$$

and for maximal twist $\omega = \pi/2$ we finally obtain:

$$\pi^0 = \frac{1}{\sqrt{2}}(\bar{u}u + \bar{d}d)\,. \tag{169}$$

References

[1] M. Creutz and B. Freedman, "A Statistical Approach To Quantum Mechanics" Annals Phys. **132**, 427 (1981)

[2] H. J. Rothe, "Lattice gauge theories: An Introduction" World Sci. Lect. Notes Phys. **74** (2005)

[3] T. DeGrand and C. E. Detar, "Lattice methods for quantum chromodynamics" *New Jersey, USA: World Scientific (2006) 345 p*

[4] M. E. Peskin and D. V. Schroeder, "An Introduction To Quantum Field Theory" *Reading, USA: Addison-Wesley (1995) 842 p*

[5] Ph. Boucaud *et al.* [ETM collaboration], "Dynamical Twisted Mass Fermions with Light Quarks: Simulation and Analysis Details" Comput. Phys. Commun. **179** (2008) 695 [arXiv:0803.0224 [hep-lat]].

[6] K. Jansen, C. McNeile, C. Michael, C. Urbach and f. t. E. Collaboration, "Meson masses and decay constants from unquenched lattice QCD" arXiv:0906.4720 [hep-lat].

[7] K. Jansen, C. Michael and C. Urbach [ETM Collaboration], "The eta' meson from lattice QCD" Eur. Phys. J. C **58** (2008) 261 [arXiv:0804.3871 [hep-lat]].

[8] R. Frezzotti and G. C. Rossi, "Chirally improving Wilson fermions. I: O(a) improvement" JHEP **0408**, 007 (2004) [arXiv:hep-lat/0306014].

[9] U. Wolff [ALPHA collaboration], "Monte Carlo errors with less errors" Comput. Phys. Commun. **156** (2004) 143 [Erratum-ibid. **176** (2007) 383] [arXiv:hep-lat/0306017].

[10] P. A. Boyle, A. Juttner, C. Kelly and R. D. Kenway, "Use of stochastic sources for the lattice determination of light quark physics" JHEP **0808** (2008) 086 [arXiv:0804.1501 [hep-lat]]

[11] B. Efron and Robert. J. Tibshirani, "An introduction to the bootstrap" *Boca Raton, USA: Chapman and Hall/CRC (1993)*

[12] A. Shindler, "Twisted mass lattice QCD" Phys. Rept. **461** (2008) 37 [arXiv:0707.4093 [hep-lat]]

[13] A. M. Sanchez, R. Welsing "Looking at the Harmonic Oscillator with Lattice field theoretical methods" DESY Summer Student Programme (2008) [http://www-zeuthen.desy.de/summerstudents/2008/doc/Welsing.pdf]